# HØJTEMPERATURKORROSION I DANSKE KRAFTVÆRKER

## CORROSION AND MATERIALS PERFORMANCE IN BIOMASS FIRED AND CO-FIRED POWER PLANTS

M. Montgomery

IPL – Materials and Process Technology
Technical University of Denmark, Building 204
2800 Lyngby, Denmark

O.H. Larsen

ELSAM Engineering
Fynsværket
Havnegade 120
5100 Odense, Denmark.

O. Biede

Energi E2
Teglholmsgade 8
2450 København SV

**Abstract**

In Denmark, biomass such as straw or wood is utilised increasingly as a fuel for generating energy. Straw combustion can give rise to specific chlorine corrosion problems not previously encountered in coal-fired power plants. The type of corrosion attack can be directly ascribed to the composition of the deposit and the metal surface temperature. In woodchip boilers, a similar corrosion rate and corrosion mechanism has on some occasions been observed. Co-firing of straw (10 and 20% energy basis) with coal has shown corrosion rates lower than those in biomass plants. With both 10 and 20% straw co-firing, no chlorine corrosion was seen. This paper summarises results from in situ investigations undertaken on high temperature corrosion in biomass fired plants. Results from 100% straw-firing, woodchip and co-firing of straw with coal will be reported. The corrosion mechanisms observed are summarised and the corrosion rates for TP347H with the different fuels are compared.

**Introduction**

In Denmark, there have been serious efforts to reduced carbon dioxide emissions by using carbon dioxide neutral fuels such as straw or wood for generating energy. For this reason, ELSAM and Energy E2 have over the past decade conducted many field investigations involving with various types of fuel combinations. Table 1 gives the data of the plants whose results are included in this paper.

Table 1: Summary of in Plant Data

| Plant Description | Steam Temp. °C | Pressure MPa | Size $MW_{th}$ |
|---|---|---|---|
| Masnedø CHP - grate-fired Almost 100% straw | 520 | 9.2 | 33 |
| Rudkøbing CHP grate-fired 100% straw | 450 | 6.1 | 10.7 |
| Maribo Sakskøbing CHP grate-fired 100% straw | 540 | 9.3 | 33 |
| Ensted CHP grate fired<br>- 100% straw boiler<br>- 100% woodchip | <br>470<br>470-540 | <br>20.1 | <br>99.4<br>16.3 |
| Studstrup suspension fired coal plant modified for coal + 20% straw | 540 | 14.3 | 380 |

Three types of corrosion investigations have been undertaken: a) exposure of metal rings on air/water cooled probes, b) exposure of test tubes in the test superheater c) exposure of test tubes in existing superheaters. The aim of the corrosion programme has been to i) measure accurately corrosion rates in existing superheaters, ii) measure corrosion rates of possible alternative materials at other temperatures. More detailed discussions of the various aspects of corrosion have been presented in previous articles [1-14].

**Straw-firing**

Many in situ corrosion investigations have been undertaken in straw-fired boilers in combined heat and power (CHP) plants. A schematic diagram showing the corrosion morphology of specimens exposed in straw-fired plants is given in Figure 1.

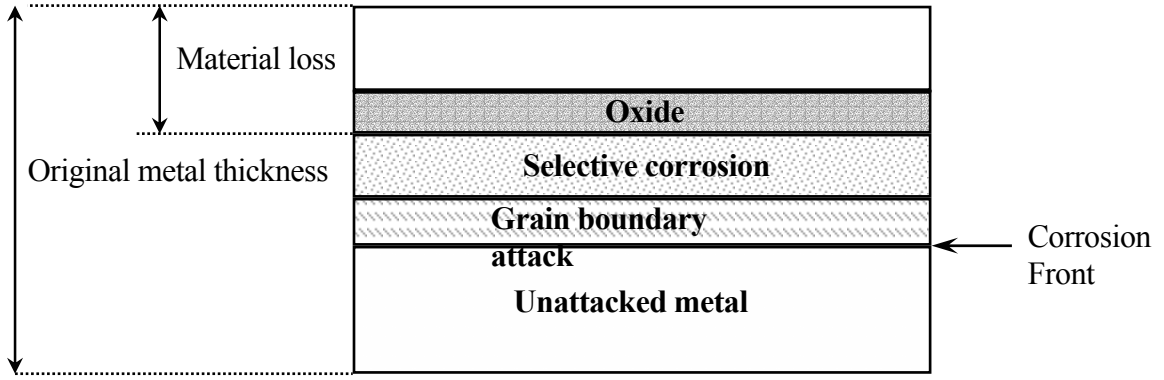


Figure 1: Schematic of corrosion attack in straw fired plants.

This schematic is especially valid for the chromium-alloyed stainless steels at high temperatures, as can be seen in Figure 2 for TP347H type steel. Note: Surface metal temperatures are used in this paper, as this gives a more relevant relation to corrosion rates than steam temperatures.

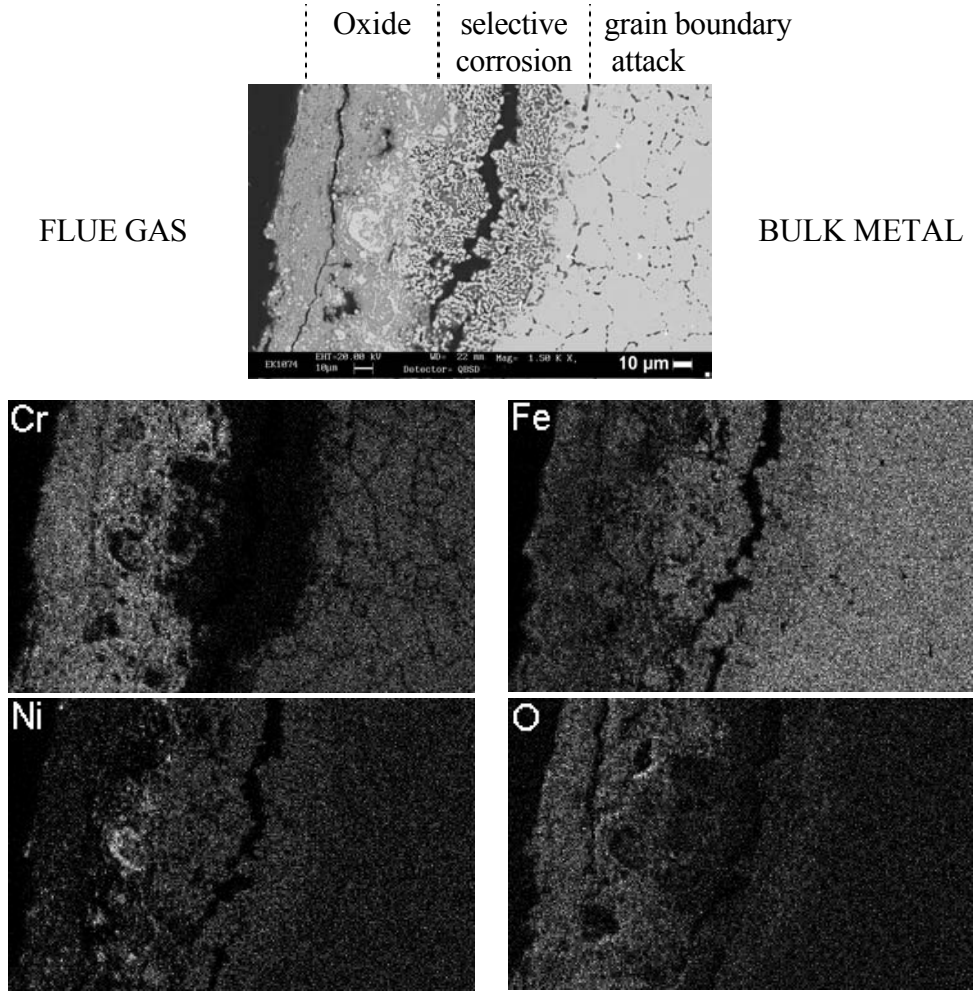

Figure 2: TP347H FG exposed for 3500 hours at Masnedø: calculated metal temperature 613°C.

Selective removal of chromium (where the metal becomes porous) and grain boundary attack is observed, such that the sum of the internal corrosion attack can be over ½ mm. For austenitic steels, grain-boundary corrosion is a precursor to corrosion within the grains. The corrosion products formed are chromium oxides and iron oxides; these are present at the surface of the specimen. In many cases, nickel is also present in the outer corrosion product as non-reacted nickel. If chlorine is detected, it is close to or at the corrosion front. No potassium is detected in this area. Even at metal temperatures lower than 500°C, chlorine containing corrosion products are still found at the corrosion front [5].

For the austenitic steels, a gradual change in the corrosion product morphology as a function of temperature is observed. A protective oxide is formed at lower surface metal temperatures below 500°C. At around 500-520°C, both grain boundary attack and protective oxides can be observed for the same specimen, as is shown for Esshete 1250. This indicates that at this temperature region, there is a transition in the type of corrosion attack (Figure 3).

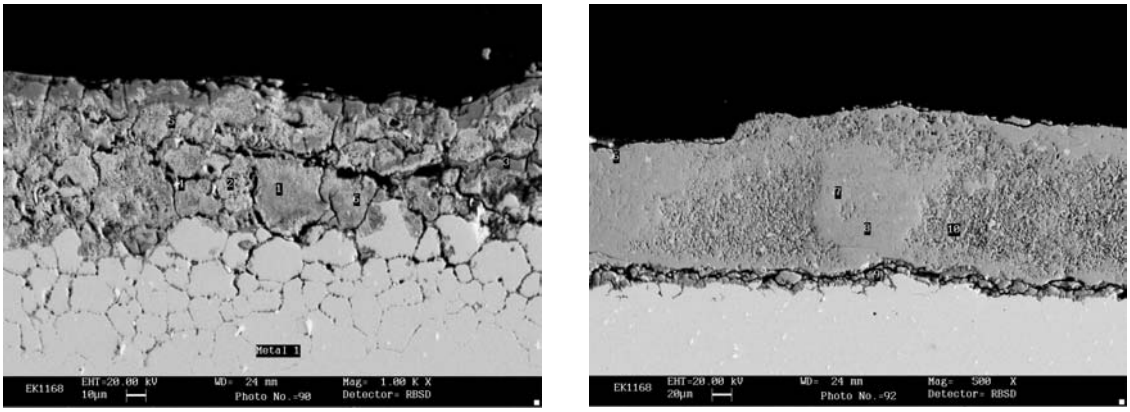


Figure 3: Two areas of the same specimen for Esshete 1250 exposed at Masnedø for 8700 h (calculated metal temperature 513°C).

Corrosion Mechanism

Initially, an outer oxide of magnetite and haematite and an inner oxide of chromium-rich iron oxide are formed at the fireside surface of the metal. Short-term deposition experiments show that potassium chloride constitutes the initial condensate on the probes [8]. Thus chlorine has to be released from these condensed deposits to result in corrosion. The initiation reaction due to the presence of potassium chloride deposits can be one or a combination of the three reactions shown below, depending on the presence of sulphur dioxide and water vapour.

$$2KCl + ½O_2 + SO_2 + H_2O \rightarrow K_2SO_4 + 2HCl \quad (1)$$

$$2KCl + O_2 + SO_2 \rightarrow K_2SO_4 + Cl_2 \quad (2)$$

$$2KCl + Fe_2O_3 + ½O_2 \rightarrow K_2Fe_2O_4 + Cl_2 \quad (3)$$

Eq. (1) releases HCl and Eq. (2) and (3) result in the release of chlorine gas. The released chlorine then migrates through the protective oxide to react at the metal-oxide interface (Eq. 4).

$$Cr + 1½Cl_2 \rightarrow CrCl_3 \quad (4)$$

A similar reaction for $CrCl_2$ would also apply. Chlorine is observed to preferentially attack chromium; this is probably due to chromium's greater affinity for chlorine than iron and nickel. The chromium chloride formed migrates out to an area of higher oxygen partial pressure and is converted to chromium oxide and chlorine (Eq. 5). Although chromium chloride has lower volatility compared to iron chloride, a temperature gradient due to the difference in metal temperature and gas temperature encourages the evaporation of metal chlorides. The released chlorine then migrates back to the corrosion front to form metal chlorides again.

$$2CrCl_3 + 1½O_2 \rightarrow Cr_2O_3 + 1½Cl_2 \quad (5)$$

Equations 4 and 5 have been termed "active oxidation" where chlorine has an almost catalytic role in converting the metal to its oxide. A similar chlorination reaction occurs for iron to form iron chloride. The precipitated chromium and iron oxide is non-protective and therefore spalls off with the ash. For austenitic materials, it is noted that grain boundaries are the initial course of attack, followed by attack of chromium within the grains. Grain boundaries present fast short-circuit diffusion paths for chlorine into the metal and chromium out of the metal. The presence of chromium carbides at grain boundaries can also lead to preferential attack [15].

Corrosion Rates

The residual unattacked metal (see Figure 1) has been measured for exposed specimens, and the corrosion rate in mm/1000h is calculated. Corrosion rates are given in mm/1000h based on the assumption that the corrosion kinetics is linear. This is clearly an acceptable assumption at the higher temperatures where non-protective oxides are present; however, at lower temperatures below 500°C, a more protective oxide is formed so the kinetics are closer to parabolic. For comparison purposes, linear kinetics has been applied.

Figure 4 shows one set of results where a range of alloys from a 2½%Cr to a 30%Cr steel were investigated at the same temperature [4].

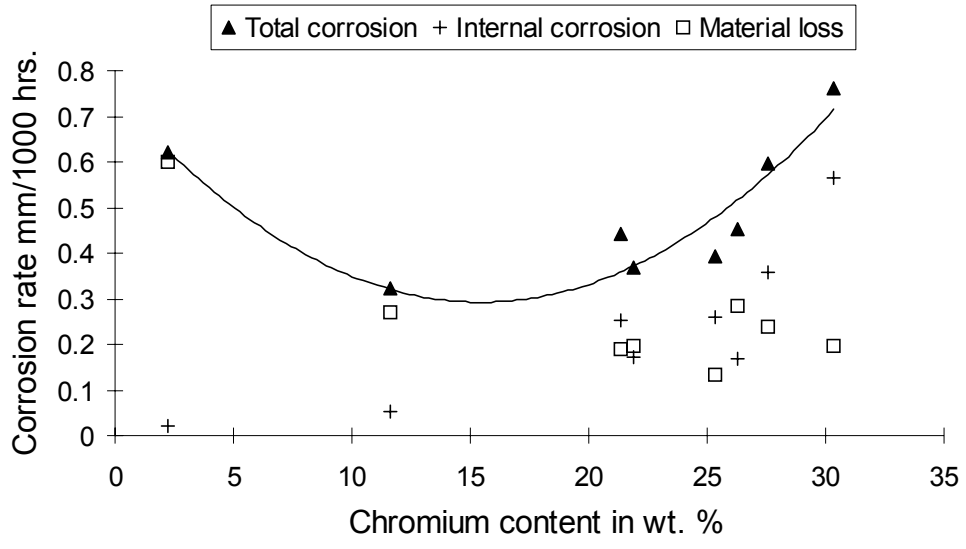

Figure 4: Corrosion rates for steels with various chromium content exposed in a probe at Masnedø straw-fired CHP Plant (approx. 550°C).

The graph shows total corrosion rate with respect to chromium percent, and also the contribution of internal corrosion (selective corrosion + grain boundary attack) and material loss to the corrosion rate. The low chromium steels exhibit a high material loss whereas the higher chromium steels are characterised by severe internal corrosion. These results indicate a minimum in total corrosion rate of steels at an intermediate chromium content of 15-18% Cr.

In Figure 5, corrosion rates for TP347H (both fine and coarse-grained) from the four straw-fired plants are collated. Both fine-grained and coarse-grained TP347H steels have similar corrosion rates. The results are illustrated on an Arrhenius type plot, with natural log of corrosion rate in mm/1000h on the y-axis and metal temperature as 1/T in Kelvin on the x-axis.

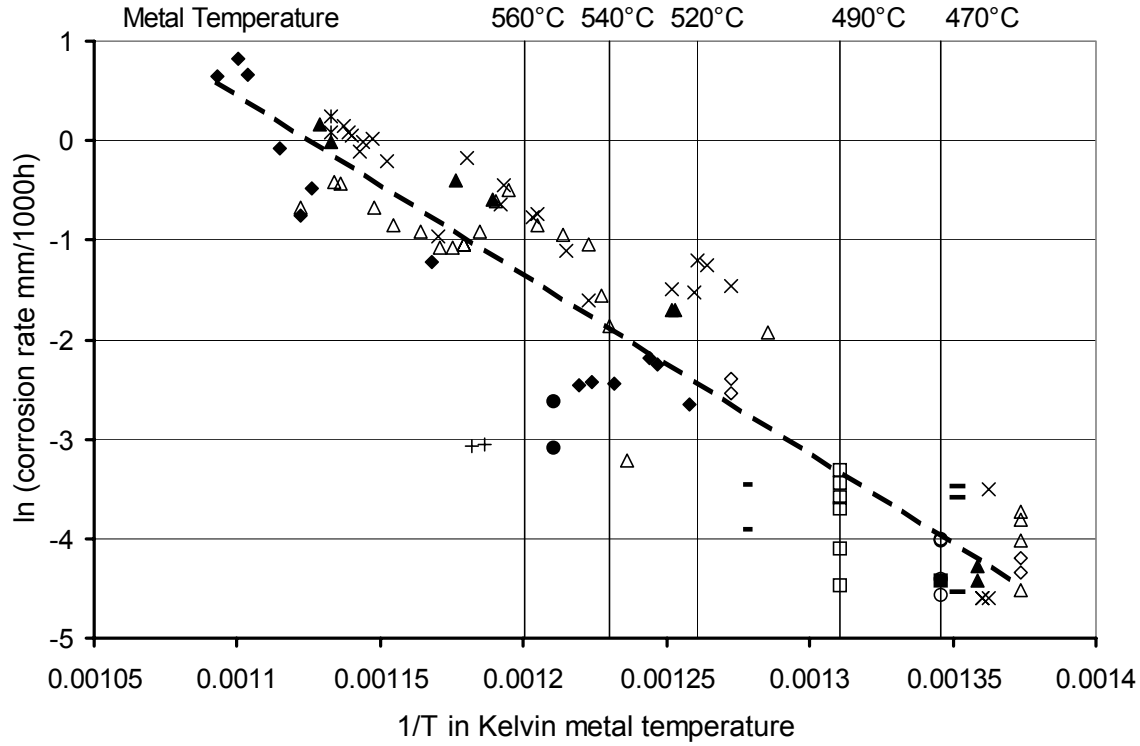


Figure 5: An Arrhenius type plot of corrosion rates for TP347H in straw-fired plants.

For test tubes in existing superheaters, the metal surface temperature is taken to be steam temperature plus 20°C, if more accurate data cannot be obtained. The corrosion rates from the four straw-fired power plants show a general agreement in results. The best-fit linear correlation has been inserted. However, there is a great spread in the results; the reasons for this are currently under investigation so that the expression for corrosion rate can be refined. Undoubtedly, a significant parameter, which has to date only been considered qualitatively, is the flue gas temperature and the heat flux [6]. Although steam temperature has been accurately measured as far as possible, measurements of gas temperatures have been incidental and less reliable.

**Woodchip Firing**

Due to the high corrosion rates experienced in straw-fired boilers, it was decided that woodchip would be a less corrosive biomass alternative. A comparison of the two fuels shows that woodchip has less ash and corrosive compounds [16]. The content of potassium and chlorine in straw is about an order of magnitude higher than in woodchip. Ensted CHP plant, commissioned in 1998, consists of a straw-fired and a woodchip boiler. The straw-fired boiler has an outlet steam temperature of 470°C. This steam is led into the woodchip boiler which has an outlet steam temperature of 540°C. The woodchip boiler is fabricated from a HCM12 steel.

Figure 6 shows TP347HFG tubes which were exposed in the plant for 2000h. In most areas, the formation of a protective oxide was seen; however, on one specimen there were areas of grain boundary attack and non-protective oxide formation. The difference in corrosion attack is also reflected in the corrosion rates where the area with protective oxide has a corrosion rate of 0.02mm/1000h, and the grain boundary attack area was four times higher.

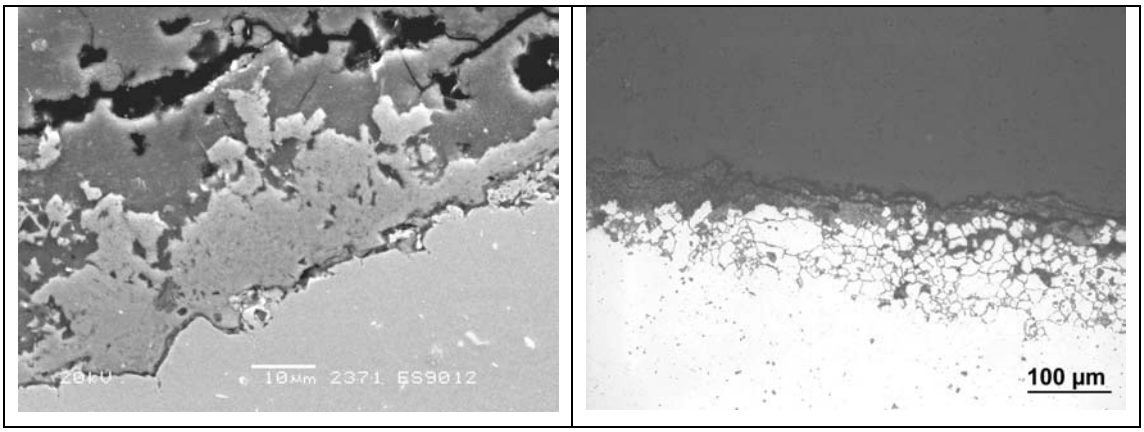


Figure 6: Two similar specimens of TP347H exposed for 2000h at the same time and location at Ensted woodchip boiler at a metal surface temperature of 520°C.

Analysis of the ash from corroded components revealed the presence of potassium sulphate and calcium sulphate close to the oxide, and in some cases potassium chloride closer to the flue gas-deposit interface. Potassium and chlorine have been detected at and near the corrosion front, which indicates that a mechanism similar to that in straw-fired boilers can occur. Where potassium chloride is in the deposit, high corrosion rates will be observed, which, in the case of TP347H, occurs as grain boundary attack similar to that in straw-fired boilers. The variability of the deposit composition leads to variable corrosion mechanisms and a difficulty in prediction of corrosion rates.

Severe corrosion problems were encountered on the panel walls at Ensted. An extensive repair procedure was carried out, consisting of weld overlay with Inconel 625 (approx. 60%Ni, 21%Cr, 9%Mo). During a boiler inspection after 6 months, a chip of Inconel 625 was removed. This chip revealed that a zone below the oxide-metal interface was depleted in chromium. An actual corrosion rate cannot be given only the depth of internal corrosion of approx. 10µm. The oxide was enriched in chromium. There was no grain boundary attack, as Inconel 625 was not a

wrought material but weld overlay. It is suggested that the corrosion attack is similar to that in straw-fired plants i.e. the depletion of chromium from the surface of the alloy by the formation of chromium chloride. The chromium chloride is then oxidised to chromium oxide. Nickel and chlorine together with oxygen were found on the surface of the material. Nickel also reacts with chlorine, however not as readily as chromium. In addition, the formation of nickel and chlorine-rich corrosion products is more stable since nickel chloride is not readily oxidised when the partial pressure of oxygen increases.

**Co-firing of coal and straw**

Due to the corrosiveness of straw, possibilities to increase electricity production from straw combustion by increasing the steam temperature is limited as this leads to unacceptable corrosion rates. ELSAM has conducted an on-site investigation at Studstrup into the feasibility of co-firing with respect to corrosion, ash deposition and aerosol formation [10]. On the basis of the positive results obtained, a co-firing plant is now in operation. The results presented here are from long-term exposures in a suspension-fired boiler with 10 and 20 % straw (% energy basis). The results are compared with those from straw-firing.

The ash adjacent to the corrosion products was investigated with SEM-EDS and the trend in Figure 7 was seen.

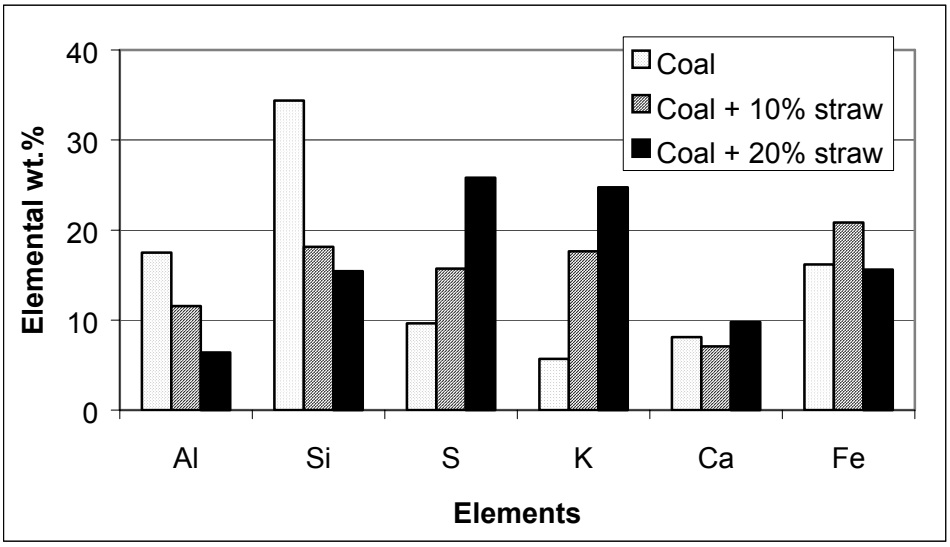


Figure 7: EDS analysis for average composition of main elements in ash adjacent to corrosion products. (Oxygen is not included in the analysis.)

The main elements detected in the ash are aluminium, silicon, sulphur, potassium, calcium and iron. Whilst aluminium and silicon decrease as the percentage of straw in fuel increases, the percentage of sulphur and potassium increases. Deposition studies support this observation [12]. No chlorine was detected in the deposits or corrosion product, or at the corrosion front. The composition of the ash showed particles rich in aluminium, silicon, potassium and oxygen (potassium aluminosilicates) in a matrix rich in potassium, sulphur and oxygen, i.e. potassium sulphate. Iron oxide precipitates were also present within this potassium sulphate matrix.

The corrosion morphology for 10% straw and 20% straw co-firing at low metal temperatures is similar to that seen in coal-firing plants, i.e. an outer layer of iron oxide, and an inner layer of iron chromium oxide. Sulphur in the form of sulphates or sulphides are present within the oxide. With 20% straw co-firing at high temperatures (approx. 580°C), as well as the corrosion morphology described above, large shallow oxide pits are present, especially for the austenitic steels. Figure 8 shows a thin and thick oxide on the same specimen of a HR3C steel (niobium modified 310 stainless steel). The thin oxide is similar to that seen with 10% co-firing for this high alloyed steel. In the base regions of the oxide pit, sulphates or sulphides are detected.

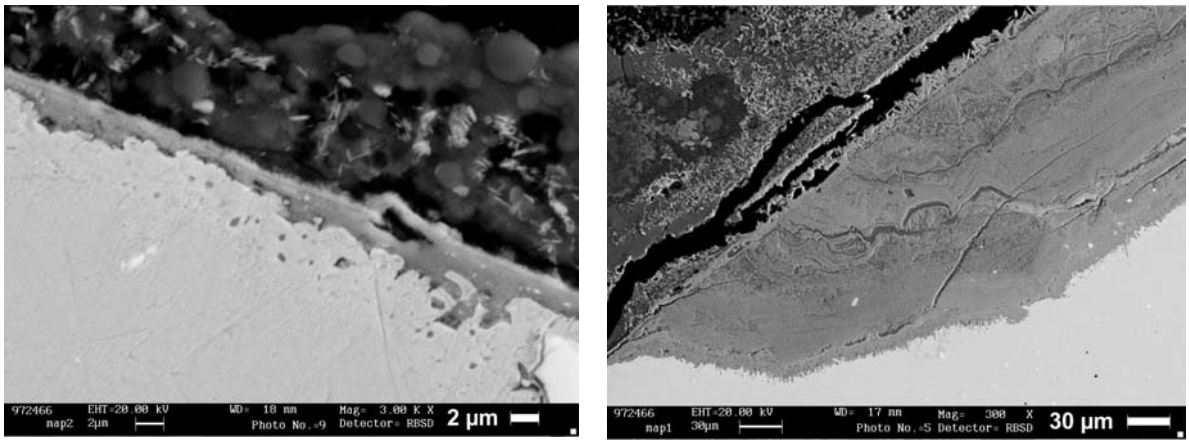


FIGURE 8 - Two different areas on the niobium modified 310 steel specimen with a metal temperature of 586°C exposed at Studstrup to 20% straw co-firing.

Corrosion Mechanism

The following corrosion mechanism is proposed. Potassium chloride from straw combustion reacts in the combustion chamber (Eq. 6 and 7) to form potassium aluminium silicates and potassium sulphate. Chlorine is released as hydrogen chloride according to the following reactions.

$$2KCl + Al_2O_3 + 6SiO_2 + H_2O \rightarrow K_2O \cdot Al_2O_3 \cdot 6SiO_2 + 2HCl \quad (6)$$

$$2KCl + SO_2 + H_2O + ½O_2 \rightarrow K_2SO_4 + 2HCl \quad (7)$$

Potassium sulphate is deposited on the metallic components together with potassium aluminosilicates. Hydrogen chloride gas is released into the flue gas. An increase in straw content from 10% to 20% results in a greater amount of potassium chloride in the combustion chamber. This is converted to more potassium sulphate (Eq.7) which deposits on the superheaters. In addition, hydrogen chloride emission from the stack increases with increase in straw percentage. [10]

In contrast to the above finding, severe chloride attack was experienced in a circulating fluidised bed (CFB) plant firing 18% straw with coal [1,14]. This difference was attributed to the differences in combustion temperature, since CFB combustion takes place at 850°C whereas in a

suspension-fired boiler, combustion temperatures are in the region of 1400-1700°C. Thus in the CFB plant, most potassium is in the form of KCl. The lower heat-up rates and lower sulphur dioxide partial pressures are not favourable for incorporation of potassium in insoluble silicates, or for major sulphation in the flue gas.

At 10% straw co-firing and at 20% straw co-firing at low temperatures, sulphidation and oxidation occur where the oxidants are supplied from potassium sulphate present in the deposit. When there is more sulphur and potassium in the deposit, i.e. with 20% co-firing, there is increased corrosion due to a greater amount of potassium sulphate salt in contact with the metal.

At 20% straw co-firing at higher metal and gas temperatures, both formation of large shallow pits and thin chromium rich oxide is observed for high alloy steels. This indicates a more corrosive environment in some localised regions. The deposit adjacent to the oxide is highly heterogeneous with aluminate and silicate particles surrounded by potassium sulphate. Corrosion increases with potassium sulphate concentration indicating that potassium sulphate is the corrosive species in the deposit. Iron oxide at the oxide-salt interface can react with sulphur trioxide to form iron sulphate (Eq. 8).

$$Fe_2O_3 + 3SO_3(g) \rightarrow Fe_2(SO_4)_3 \quad (8)$$

The phase diagram of a eutectic melt of iron sulphate and potassium sulphate gives a melting point of 621°C and contains approximately 90 mol.% potassium sulphate [17]. There are two criteria that have to be fulfilled to result in the presence of a ferric sulphate-potassium sulphate eutectic melt. The ash must have a high potassium sulphate concentration and the temperature of the melt must be close to the eutectic melting point. At 20% co-firing at metal temperatures of 580°C, there is a high concentration of potassium sulphate, and it is assumed that the temperature at the oxide-deposit interface is sufficient to form a eutectic melt. Based on simultaneous thermal analysis (STA), a mixture of potassium sulphate and haematite has the first melt phases at 586°C [8]. Trace amounts of other elements might also give a sub-cooling effect so that the temperature of the eutectic melt is lowered. It is therefore suggested that low temperature hot corrosion [18] occurs at the higher temperatures with 20% straw co-firing. Thus iron sulphate forms a melt with potassium sulphate, and due to $SO_3$ gradients, iron sulphate will migrate to the outer part of the melt and precipitate haematite. The net result is that at high temperatures of 580-600°C, the presence of potassium sulphate leads to acidic fluxing of haematite.

Corrosion Rates

Co-firing in a suspension-fired boiler with either 10% or 20% straw removes the danger of catastrophic chlorine corrosion. The corrosion rate is much lower than that seen in straw-fired

power plants and is closer to that in coal-fired power plants. For comparison purposes, the corrosion rates for TP347H FG have been plotted with respect to metal temperature (Figure 9).

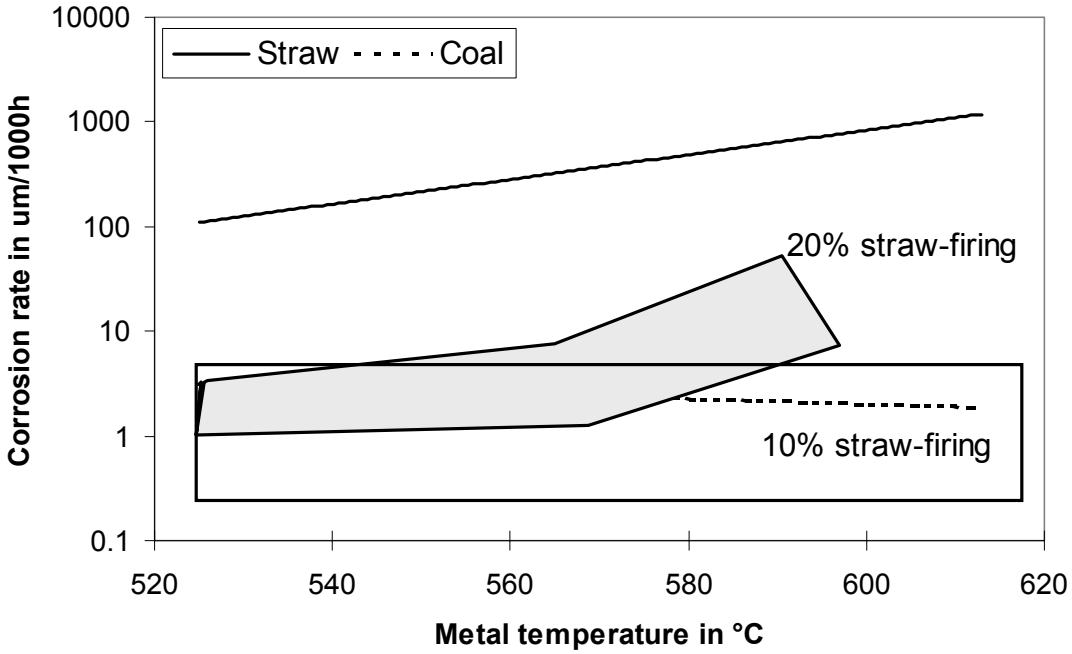


Figure 9: Comparison of TP347H corrosion rates in co-firing of straw and coal compared to 100% coal-firing and 100% straw-firing.

Corrosion rates in straw co-firing lie in the same region as those for coal-firing and significantly below the results for straw-firing. For specimens with 10% straw co-firing, corrosion rates can be considered as similar to coal-firing in all temperature ranges, even those where there is an increased metal temperature. For 20% straw co-firing at low temperatures, the corrosion rate is also similar to coal-firing. There is an increase in the corrosion rate at high temperatures due to the change in corrosion mechanism as iron sulphate-potassium sulphate melt is formed.

**Conclusions**

1. In straw-fired boilers, high corrosion rates are observed due to the presence of potassium and chlorine rich deposits. At high temperatures, a chlorination reaction occurs where the alloy is attacked first at the grain boundaries followed by chromium depletion within the grains.
2. Experience from woodchip fired boilers indicates also the threat of chlorine corrosion due to a similar mechanism as in straw-fired plants. However, there are variations in corrosion rates, which is probably related to the heterogeneous character of the deposits.
3. In co-firing with coal and 10 - 20 % straw (on energy basis), chlorine corrosion is not seen. Potassium sulphate in the deposit is the corrosive specie. The corrosion rates for TP347H are significantly below those from 100% straw-firing, and closer to those in coal-fired power

plants. At 20% straw co-firing at high temperatures, the corrosion rates increase due to a change in corrosion mechanism, however they are still below those for straw-firing.

It must be noted that corrosion rates in this paper are specific to the investigations conducted at the plants in Denmark. The results described here are dependent on the coal and biomass type utilised.

**Acknowledgements**

Part of this work has been funded by PSO (public service obligations) through ELTRA and Elkraft Systems.

**References**

1. O.H. Larsen and N. Henriksen, Proc. Power Plant Technology, Kolding 4-6 Sept. pp 7.1-7.18. (1996)
2. N. Henriksen et al, VGB Conference Corrosion and Corrosion Protection in Power Plants 1995.
3. N. Henriksen and O.H. Larsen, Materials at High Temperatures, 14 (3) pp. 227-236 1997
4. M. Montgomery and A. Karlsson, Materials and Corrosion, 50 579-584 (1999)
5. M. Montgomery, A. Karlsson and OH Larsen, Materials and Corrosion 53 pp. 121-131 (2002).
6. M. Montgomery, O. Biede and OH Larsen, Materials for Advanced Power Engineering 2002 Part II pp 957-966 (2002).
7. M. Montgomery, B. Carlsen, O. Biede and OH Larsen Proc. NACE Conference CORROSION/2002, paper 02379.
8. H.P. Nielsen, Ph.D Thesis, Technical University of Denmark, (1998).
9. N. Henriksen, M. Montgomery and O.H. Larsen, Korrosion in energieerzeugenden Anlagen VDI-Berichte 1680. VDI Verlag GmbH Düsseldorf pp 111-133 (2002).
10. K. Wieck Hansen, P. Overgaard, O.H. Larsen, Biomass and Energy, 19 pp 395-409 (2000).
11. M. Montgomery and O.H. Larsen, Materials and Corrosion, 53 pp185-194 (2002).
12. K.H. Andersen, Ph.D Thesis, Technical University of Denmark 1998.
13. M. Montgomery, O. Biede, OH Larsen, Proc. NACE conference CORROSION/2003 paper 03356
14. N. Henriksen and P.F.B. Binderup, CFB Material Test at Grenaa CHP Plant, Internal Report 1995.
15. D.A. Berztiss et al Z. Metallkd. 90 pp.4-12 (1999).
16. B. Sander, Biomass and Bionergy, 12 3 pp177-183, (1997)
17. A. Rahmel: VGB Mitteilungen 74 October (1961).
18. R.A. Rapp, Materials Science and Engineering 87 pp 319-327 (1987).